The Compact Muon Solenoid Experiment

Analysis Note

The content of this note is intended for CMS internal use and distribution only

September 10, 2009

Search for New Particles Decaying to Dijets in pp Collisions at $10\ TeV$

Sertac Ozturk

University of Cukurova, Adana, Turkey

Visitor at Fermilab, Batavia, IL, USA

Robert M. Harris and Konstantinos Kousouris

Fermilab, Batavia, IL, USA

Chiyoung Jeong and Sung-Won Lee

Texas Tech University, Lubbock, TX, USA

Abstract

This note is intended as documentation for draft paper QCD-09-006. We use a simulated pseudo-data sample corresponding to $10\ pb^{-1}$ of integrated luminosity from the CMS experiment at a collision energy of 10 TeV to test our plans to search for new particles decaying to dijets. We describe the planned search analysis and its systematic uncertainties. By construction the measured dijet mass spectrum in this test agrees with the QCD prediction. Applying our search to this sample, we exclude at 95% confidence level models containing the following particles: axigluon and flavor universal coloron with mass below $1.8\ TeV$, excited quarks with mass below $1.8\ TeV$ and E_6 diquark with mass below $1.0\ TeV$ and mass between $1.3\ TeV$ and $1.7\ TeV$.

1 Introduction

1.1 Theoretical Motivation

The Standard Model (SM) is the current theory of quarks and leptons and their electromagnetic, weak, and strong interactions. However, it is not a complete theory because it has important unanswered questions, such as: Why do quarks come in different flavors? Why are the quarks arranged in generations? Why are there four different forces? How do we unify gravitation with the other forces? Why is gravity so weak?

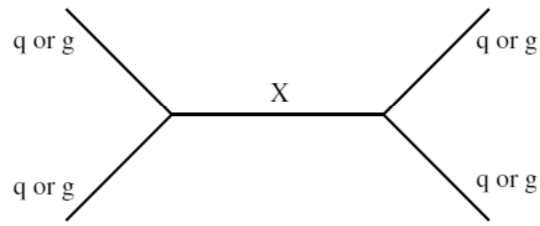

Figure 1: Feynmann Diagram of dijet resonance.

There are new theories that try to address these questions. As these theories try to answer these unanswered questions, they often predict extremely short-lived particles called resonances. Theoretical ideas behind the concepts of technicolor and extended technicolor attempt to explain the reason and origin for different quark flavors. They predict two new resonances named color octet technirho [1] and coloron [2]. Compositeness explains the reason behind quark families by proposing a composite structure for quarks and postulates the existence of excited quarks [3]. Grand unified theories address the question Why are there different forces? and in doing so, require new heavy Z and W bosons [4]. The unification of gravity with other fundamental forces is generally dealt with by string theories. Some superstring models predict that at low energies the SM originates from the E6 gauge group that contains diquarks [5]. The theory of extra dimensions attempts to explain the reason why gravity is so weak. It postulates that the strength of gravity is reduced by leaking into an extra dimension and predicts a new particle called graviton [6].

Model Name	X	Color	J^P	$\Gamma/(2M)$	Chan
Excited Quark	q*	Triplet	$1/2^+$	0.02	qg
E_6 Diquark	D	Triplet	0^+	0.004	qq
Axigluon	A	Octet	1^+	0.05	$q\bar{q}$
Coloron	C	Octet	1^-	0.05	$q\bar{q}$
RS Graviton	G	Singlet	2^-	0.01	$q\bar{q}$, gg
Heavy W	W'	Singlet	1^-	0.01	$q\bar{q}$
Heavy Z	Z'	Singlet	1^-	0.01	$q\bar{q}$

Table 1: Resonance Models

1.2 Experimental Technique

QCD dijet events are dominant process in a hadron collision. Our experimental method for dijet resonance is to search in dijet mass spectrum. If a resonance exist, it can appear in dijet mass spectrum as a bump.
The process of $q* \to qg$, $G \to q\bar{q}$ and $G \to gg$ were simulated using PHYTIA [11] as resonance signals. Then, we produced a pseudo-data as a Background for our search. A toy generator was written to produce random statistical fluctuation in smooth QCD background curve. It gave us a pseudo-data sample look like real data at $10pb^{-1}$ of integrated luminosity and we used it for dijet resonance search. To calculate the upper cross section limit, we perform a binned maximum likelihood method [7]. The method gives a Poisson likelihood as a function of the cross section. Then we calculate the 95% confidence level upper limit on the cross section including only statistical uncertainties. Then, we convulate likelihood distribution with Gaussian and 95% confidence level upper limit on the cross section is found including systematic uncertainties.

2 Definition of Jets and Dijet Mass Spectrum

Within the standard model events with two energetic jets (dijets) are expected to arise in proton-proton collisions from parton-parton scattering. The outgoing scattered partons manifest themselves as hadronic jets. The pseudorapidity, η, of the observed jets is predicted by the angular distribution of the scattered partons in Quantum Chromodynamics (QCD).

Jets are reconstructed using the seedless infrared safe cone algorithm with cone size $R = \sqrt{(\Delta\eta)^2 + (\Delta\phi)^2} = 0.7$ [8]. Below we will discuss three types of jets: reconstructed, corrected and generated. The reconstructed jet energy, E, is defined as the scalar sum of the calorimeter tower energies inside the jet. The jet momentum, $\vec{p}$, is the corresponding vector sum: $\vec{p} = \sum E_i \hat{u}_i$ with $\hat{u}_i$ being the unit vector pointing from the origin to the energy deposition E_i inside the cone. The jet transverse momentum, p_T, is the component of $\vec{p}$ in the transverse plane. The E and $\vec{p}$ of a reconstructed jet are then corrected for the non-linear response of the calorimeter to a generated jet. Generated jets come from applying the same jet algorithm to the Lorentz vectors of stable generated particles before detector simulation. The corrections are chosen so that, on average, the p_T of a corrected jet is equal to the p_T of the corresponding generated jet. More details on jet reconstruction and jet energy corrections can be found in [9, 10].

The dijet system is composed of the two jets with the highest p_T in an event (leading jets), and the dijet mass is given by $m = \sqrt{(E_1 + E_2)^2 - (\vec{p}_1 + \vec{p}_2)^2}$. For both leading jets required to have pseudorapidity $|\eta| < 1.3$. The sample we use for this search was collected by requiring at least one jet in the high level trigger with $p_T > 110$ GeV/c. The trigger efficiency, measured from a sample acquired with a prescaled trigger with a lower p_T threshold, was greater than 99% for dijet mass above 420 GeV/c^2. Backgrounds from cosmic rays, beam halo, and detector noise are expected to occasionally produce events with large or unbalanced energy depositions. They are removed by requiring $\not{E}_T / \sum E_T < 0.3$ and $\sum E_T < 10$ TeV, where $\not{E}_T$ ($\sum E_T$) is the magnitude of the vector (scalar) sum of the transverse energies measured by all calorimeter towers in the event. This cut is more than 99% efficient for both QCD jet events and the signals of new physics considered. In the high p_T region relevant for this search, jet reconstruction is fully efficient. Then, the dijet mass spectrum is formed as follows;

$$\frac{d\sigma}{dm_{jj}} = \frac{1}{\int Ldt} \frac{N_i}{\Delta m_{jj}} \tag{1}$$

where N_i is the number of events in the i-th dijet mass bin, Δm_{jj} is the i-th dijet mass bin width.

In Fig. 2 we present the inclusive dijet mass distribution for $pp \to 2jets + X$, where X can be anything including additional jets. We plot the diffential cross section versus dijet mass in bins approximately equal to the dijet mass resolution. The black curve is smooth QCD curve from PYTHIA+CMS simulation. The data points are produced around this smooth QCD curve with statistical fluctuation. The band shows the systematic uncertainties on the data and the dashes line shows next-to-leading order QCD calculation.

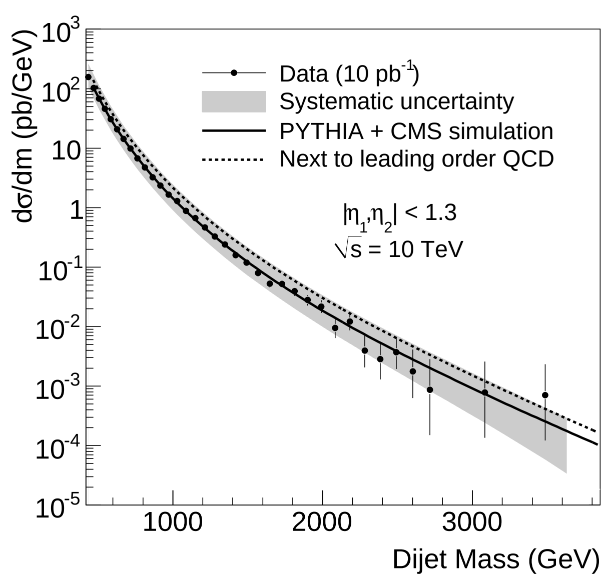

Figure 2: The dijet mass distribution compared to simulation and NLO QCD calculation.

2.1 The Signal: Dijet Resonances

The process of $q* \to qg$, $G \to q\bar{q}$ and $G \to gg$ were produced using PYTHIA [11]+CMS simulation at three different masses of $0.7\ TeV$, $2\ TeV$ and $5\ TeV$. The Fig. 3 shows the dijet mass distribution of excited quark for GenJets, CaloJets and Corrected CaloJets at three different resonance masses. The peaks of GenJets and Corrected CaloJets are expected resonance mass. The low mass tail at resonance shape comes from FSR (Final State Radiation) and high mass tail comes from ISR (Initial State Radiation).
Dijet mass resolution as a function of resonance mass is illustrated in Fig. 4. The resolution is calculated as $Sigma/Mean$ which are obtained from gaussian fit of dijet mass distribution. It is well fit by function of

$$\frac{\sigma}{Mean} = 0.042 + \frac{31.7}{M_{Res}} \tag{2}$$

where M_{Res} is resonance mass. The resolution varies from $\%10$ at $0.7\ TeV$ to $\%5$ at $5\ TeV$ and consistent with previous study [14].
In Fig. 5, we present the resonance shapes which come the process of $q* \to qg$, $G \to q\bar{q}$ and $G \to gg$ at three different masses of $0.7\ TeV$, $2\ TeV$ and $5\ TeV$. Because of different detector responce, ISR and FSR, the resonance shapes are different. The width of dijet resonances increases with number of gluon because gluons emit more radiation than quarks.

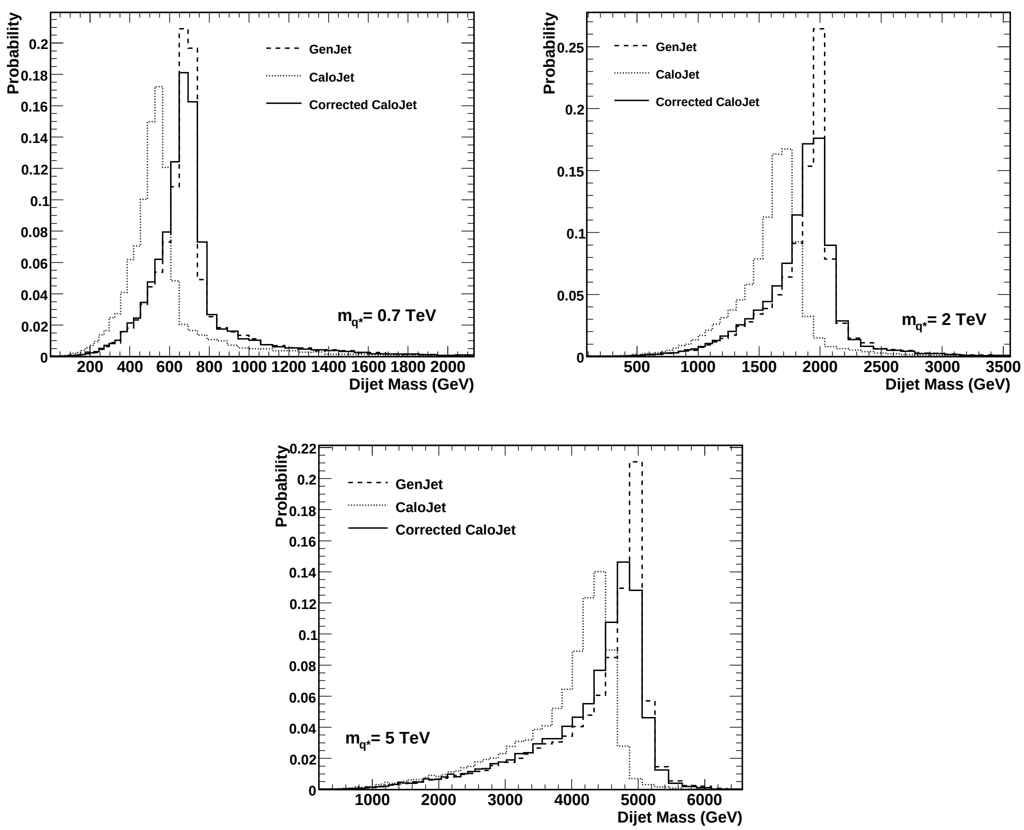

Figure 3: Dijet mass distribution for excited quark of mass at $0.7\ TeV$ (left plots), $2\ TeV$ (middle plots), and $5\ TeV$ (right plots), for GenJets, CaloJets and Corrected CaloJets.

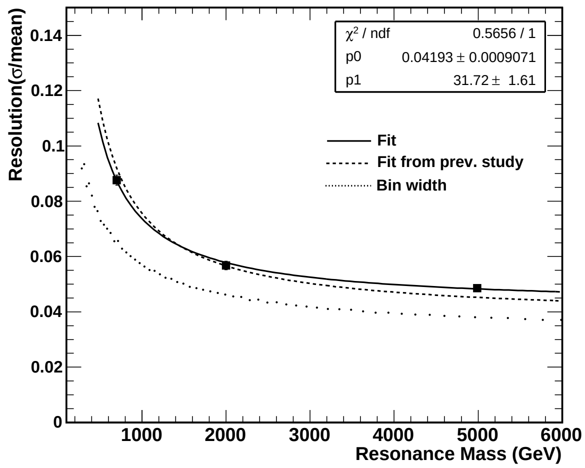

Figure 4: The dijet mass resolution as a function of resonance mass.

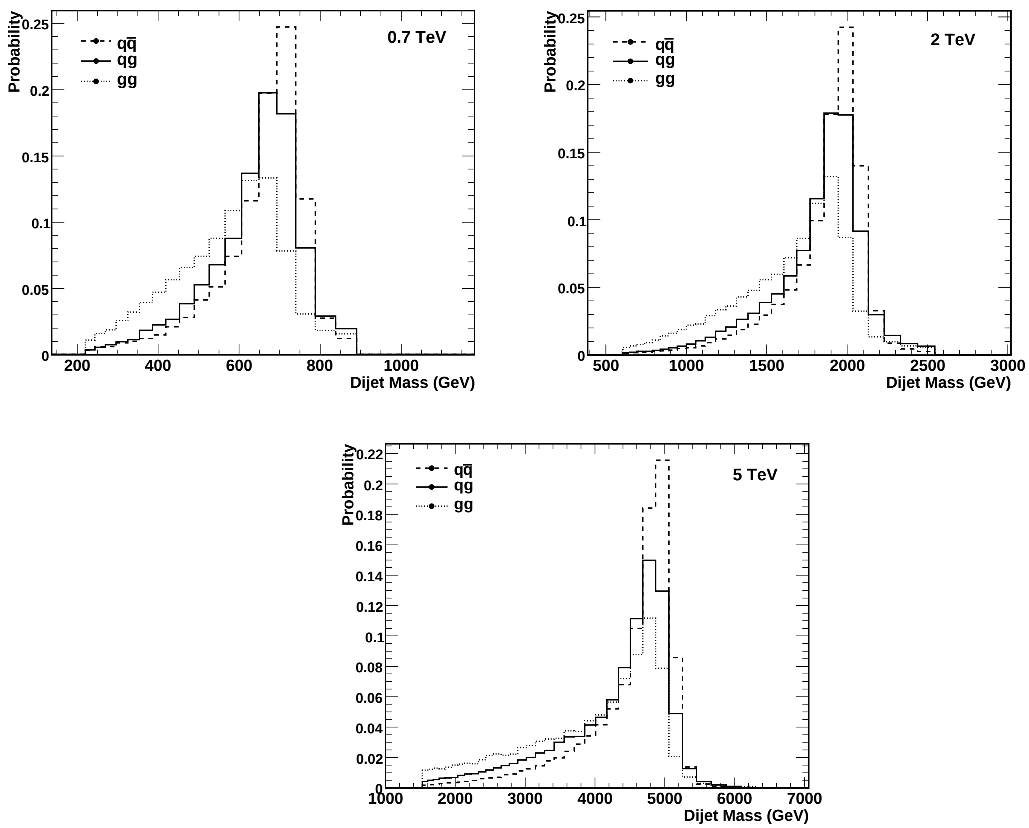

Figure 5: Dijet mass distribution for $q\bar{q}$ (qq), qg and gg resonances of mass at $0.7\ TeV$ (left plots), $2\ TeV$ (middle plots), and $5\ TeV$ (right plots).

The resonance shape in intermediate steps between generated resonance masses are obtained using interpolation technique. First, we defined a new parameter as $x = \frac{M_{jj}}{M_{Res}}$ where M_{jj} is dijet mass and M_{Res} is resonance mass. Then we generated the X distribution of any resonance mass between generated Monte Carlo resonance masses. For example, If we want to generated X distribution of mass at $1TeV$, we use the equation in below. Since $1\ TeV$ is between $0.7\ TeV$ and $2\ TeV$, we used the MC sample masses at $0.7\ TeV$ and $2\ TeV$. It gives probability in each X bins of mass at $1TeV$. Finally, X distribution was converted to variable dijet mass bins using interpolation technique to get resonance shape at any resonance masses.

$$Prob_{m=1TeV}(x) = Prob_{m=0.7TeV}(x) + \left[Prob_{m=2TeV}(x) - Prob_{m=0.7TeV}(x)\right] \cdot \frac{1-0.7}{2-0.7} \tag{3}$$

Fig. 6 shows the X distribution at $0.7\ TeV$, $2\ TeV$ and $5\ TeV$ from MC samples on the left side. The comparison of X distribution between $0.7\ TeV$, $1\ TeV$ and $2\ TeV$ is illustrated on the right side. The X distribution at $1\ TeV$ is between $0.7\ TeV$ and $2\ TeV$ as expected.
Fig. 7 shows the resonance shape of excited quark. The resonance shapes with solid lines come from Monte Carlo (MC) samples. The dashed lines show the resonance shape generated by interpolation technique for excited quark of mass at $1\ TeV$, $3\ TeV$ and $4\ TeV$. It can be seen clearly that interpolation technique is consistent with MC samples. We use these resonance shape to calculate cross section upper limit at any resonance mass.

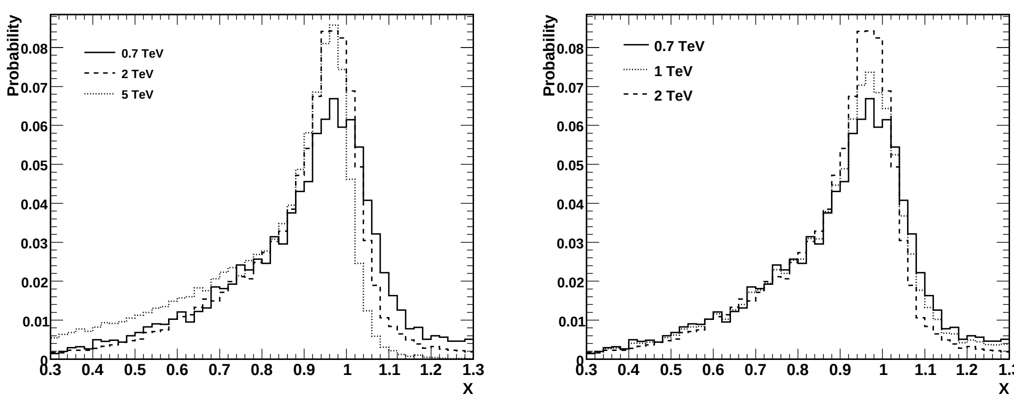

Figure 6: X distribution for excited quark of mass at $0.7\ TeV$, $2\ TeV$ and $5TeV$ (left plot). X distribution of mass at $1\ TeV$ compared with mass at $0.7\ TeV$ and $2\ TeV$ (right plot).

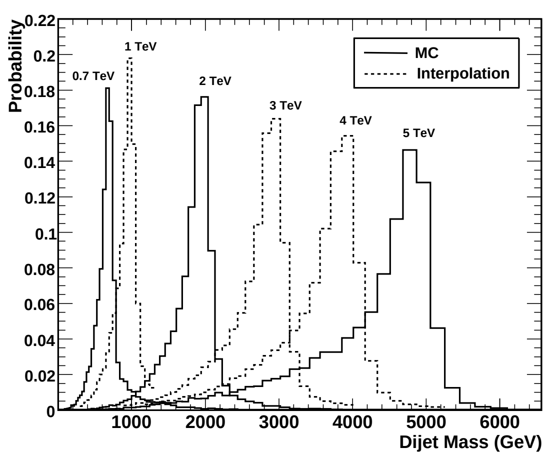

Figure 7: Resonance shapes at various resonance masses using interpolation technique compared with MC samples.

2.2 The Background: QCD Dijet

All QCD dijet events is considered background. Inclusive dijet production $(pp \rightarrow 2jets + X)$ is the most dominate process by QCD scattering of partons and QCD dijet events are the biggest background for dijet resonance search study. We generated a pseudo-data set with statistical fluctuation in smooth QCD background curve which already was discussed in Section 2. Fit function with four parameter was chosen as equation 3. We get a reasonable χ^2 of 23 for 32 degrees of freedom.

$$\frac{d\sigma}{dm} = p_0 \frac{(1 - \frac{m}{\sqrt{s}} + p_3(\frac{m}{\sqrt{s}})^2)^{p_1}}{(m/\sqrt{s})^{p_2}} \tag{4}$$

In Fig. 8, we present three different plots. The top plot in Fig. 8 shows the differential cross section of excited quark signals as a function of dijet mass with background fit. The bottom left plot shows fractional differences between data and fit function. The pulls which is defined as *(Data-Fit)/Error* are consistent with statistical fluctuations and oscillating around zero. Pseudo-data is compared to the smooth background fit and to resonance signals in bottom right side of Fig. 8. *(Data-Fit)/Fit* plot as a function of dijet mass shows that q* signals with resonance mass is less than 2 TeV could be seen or excluded.

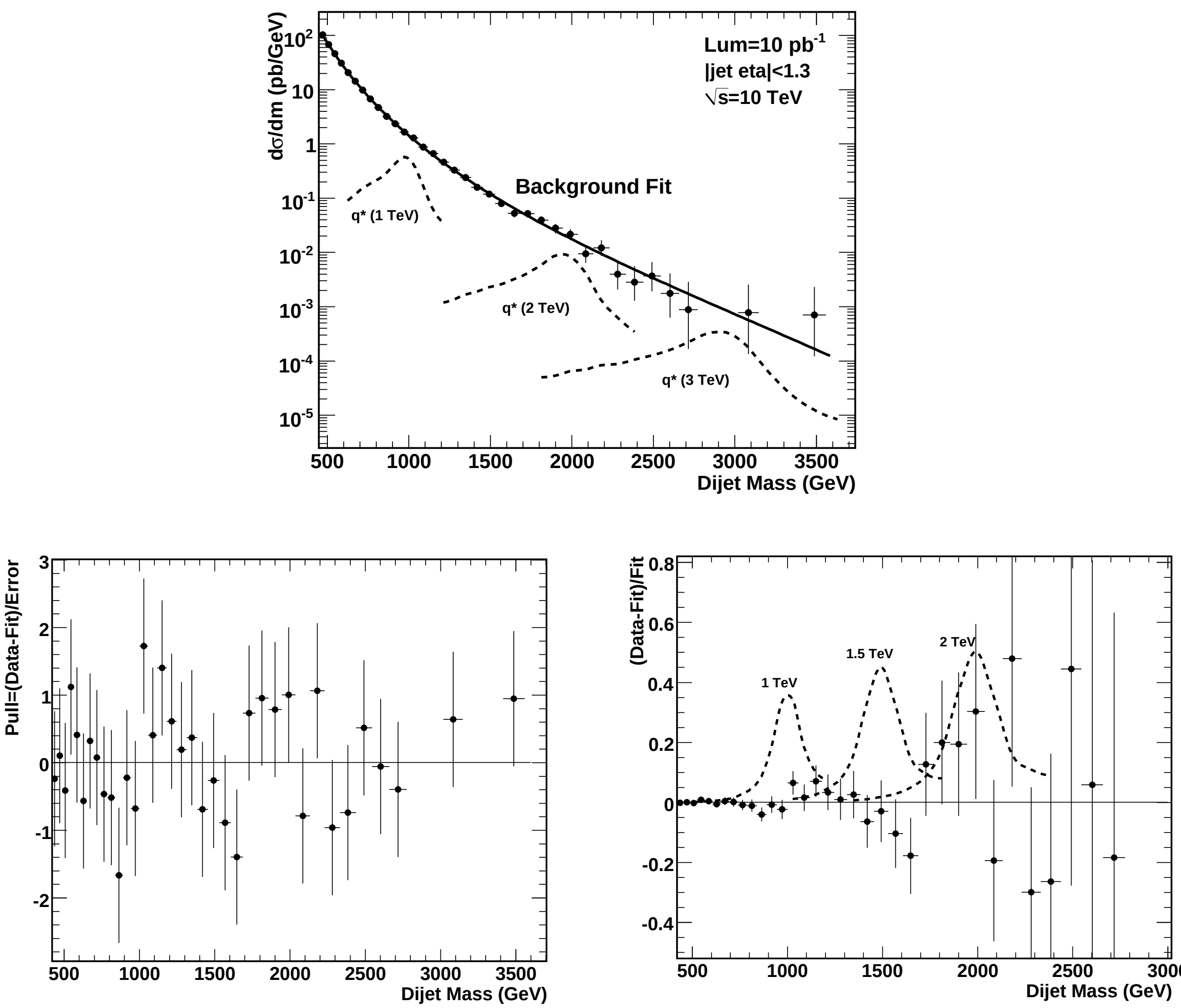

Figure 8: *The top plot*: The dijet mass distribution (points) compared to a smooth background fit (solid curve) and to a simulation of excited quarks signals in the CMS detector (dashed curves). *The bottom left plot*: (Data-Fit)/Error versus dijet mass is shown. *The bottom right plot*: The fractional difference between the dijet mass distribution (points) and a smooth background fit (solid line) is compared to simulations of excited quark signals in the CMS detector (dashed curves).

3 Search for Dijet Resonance

Bayesian technique based on binned likelihood [7] is used to calculate the limits on new particle production. The likelihood as a function of a constant can be written as:

$$L = \prod_i \frac{\mu_i^{n_i} e^{-\mu_i}}{n_i!} \tag{5}$$

where

$$\mu_i = \alpha N_i(S) + N_i(B). \tag{6}$$

n_i is measured number of events in the $i-th$ dijet mass bin, $N_i(S)$ is number of events from signal in the $i-th$ dijet mass bin, α is a constant to multiply the signal and $N_i(B)$ is number of expected events from background in the $i-th$ dijet mass bin. We consider that QCD background is fixed to the best $Signal+QCD$ fit to data point and it gives the expected number of background event in the $i-th$ dijet mass bin,$N_i(B)$. The number of signal in the $i-th$ dijet mass bin,$N_i(S)$,comes from developed interpolation technique. The signal range is chosen from $0.3 \cdot M_{Res}$ to $1.3 \cdot M_{Res}$ since high and low mass tail is affectively lost in QCD background. Then we plot likelihood distribution as a function of signal cross section for resonances with mass from $0.7TeV$ to $3.5TeV$ in $0.1TeV$ steps, and the 95% confidence level upper limit is calculated as follows;

$$\frac{\int_0^{\sigma_{95}} L(\sigma) d\sigma}{\int_0^{\infty} L(\sigma) d\sigma} = 0.95 \tag{7}$$

3.1 Upper Cross Section Limit with Statistical Error

We calculated 95% confidence level upper limit for resonances of $q\bar{q}$ (or qq), qg and gg. Fig. 9 compares the cross section limit with statistical uncertainties only to calculated resonance cross section for six different models. The bump around $1TeV$ and $2TeV$ is caused by fluctuations with low significance in the data around the same mass ranges. In Fig. 10, Likelihood distribution at various resonance masses for qg resonances are illustrated. When resonance mass increases, the 95% C.L. upper cross section limits are getting lower.

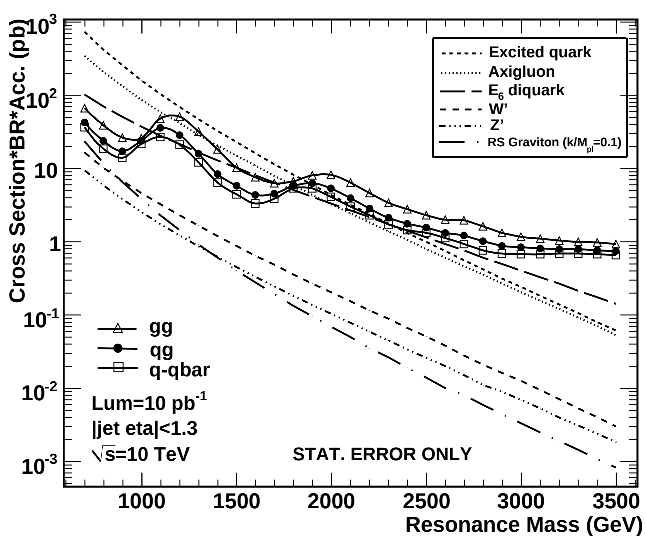

Figure 9: Dijet resonance sensitivity for 10 pb^{-1}. 95% C.L. is compared to the cross section for various resonance models. This sensitivity contains statistical error only.

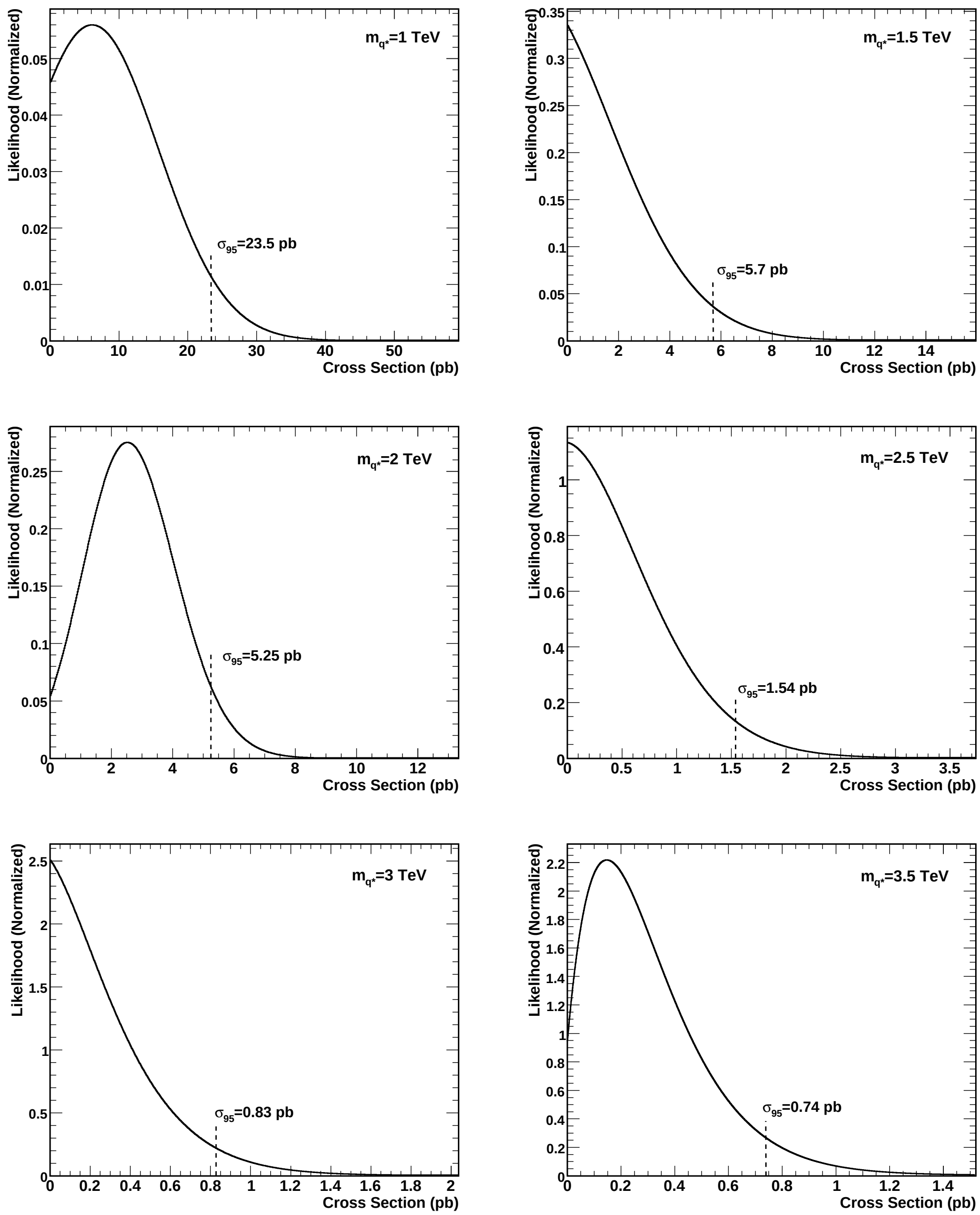

Figure 10: Likelihood distribution with %95 C.L. cross section limit at various resonance masses for excited quark resonances (Statistical error only).

3.2 Systematic Uncertainties

The source of systematic uncertainties are considered as following:

- Jet energy scale (JES)
- Background parametrization
- Luminosity

Jet Energy Scale (JES): The uncertainty on JES is basically relatively error between simulation and real data. We assume that the uncertainty on JES is roughly $\pm 10\%$ and the signal is shifted as 10% at startup. It gives more background and finding resonance signal is harder.
The left plot in Fig. 11 shows smooth cross section limit without systematics and with systematics on JES uncertainty for qg resonance. To get smooth cross section limit curve, expected events from background, $N_i(B)$, which is smooth and comes from fit function are considered as measurement number of events, n_i, in the $i-th$ dijet mass bin. Fractional change between smooth limits are illustrated separately for $q\bar{q}$ (or qq), qg and gg resonances at right plot of Fig. 11. The uncertainty on JES varies roughly from 45% at $0.7\,TeV$ to 30% at $3.5\,TeV$.

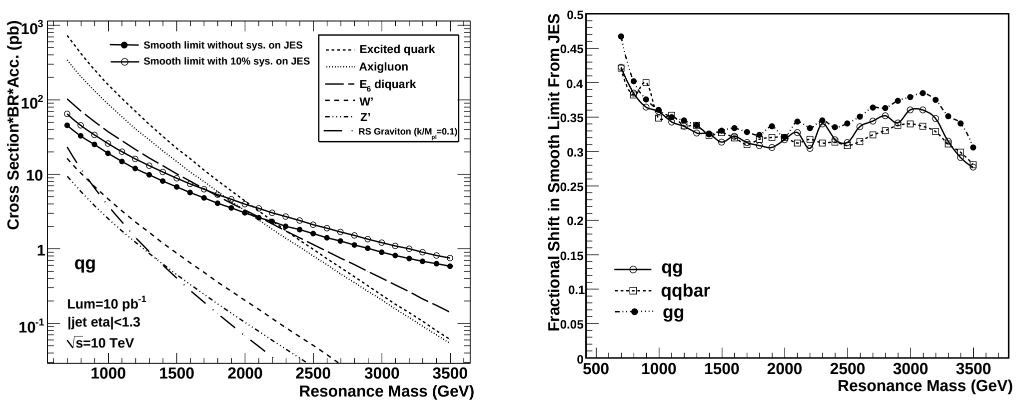

Figure 11: *Left plot*: Comparison of smoothed cross section limit without systematics and with systematic on JES uncertainty. *Right plot*:Fractional change on limit with JES systematic uncertainty.

Background Parametrization Systematic: We considered the others functional forms with 3 and 4 parameters to parameterize the QCD background. Both functional forms were used by CDF [15].

$$\frac{d\sigma}{dm} = p_0 \frac{(1-X)^{p_1}}{X^{p_2}} \tag{8}$$

$$\frac{d\sigma}{dm} = p_0 \frac{(1-X)^{p_1}}{X^{p_2+p_3 ln(X)}} \tag{9}$$

where $X = \frac{m_{jj}}{\sqrt{s}}$. Fig. 12 show comparison of fits with the data points. We found the 3 parameter form gaves the largest fractional change and we used it for Background Parametrization Systematic. The right plot in Fig. 12 presents absolute fractional change on limit for qg resonances. We smoothed the statistical variations in the absolute change in the limit with quadratic fit. Systematic uncertainty varies from 8% at $0.7\,TeV$ to 40% at $3.5\,TeV$. The same effect is observed for $q\bar{q}$ (or qq) and gg resonances.

Luminosity: We assumed the uncertainty on luminosity about 10% at startup.

We determine 1σ change for each systematic uncertainty in signal that we can discovery or exclude. To find total total systematics, we add the these 1σ changes as quadrature. The individual and total systematic uncertainties as a function of resonance mass are illustrated in Figure 6. Absolute uncertainty in each resonance mass is calculated as total systematics uncertainty multiply by upper cross section limit.

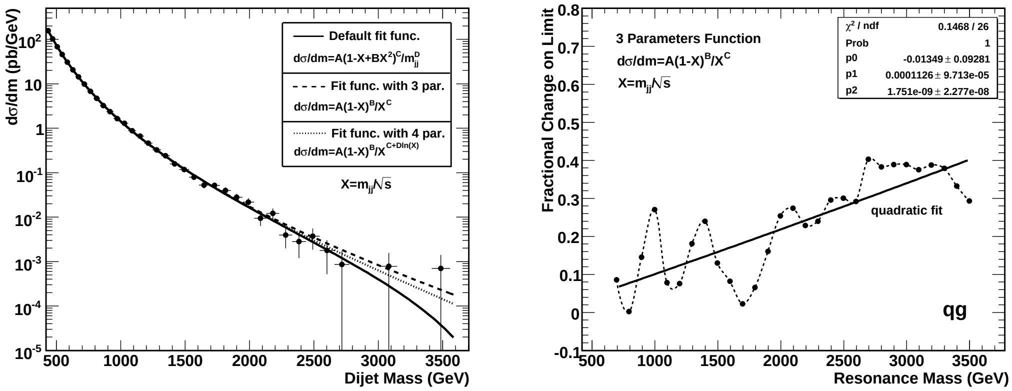

Figure 12: *Left plot*: Comparison of fit functions for background parametrization. *Right plot*:Absolute fractional change on limit with smooth quadratic fit.

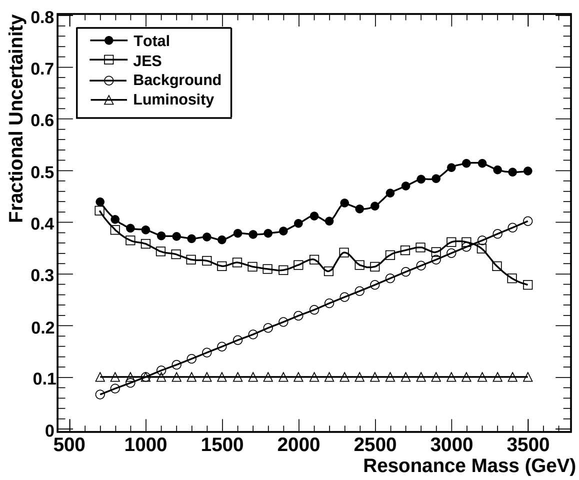

Figure 13: Fractional systematic uncertainties on signal cross section.

3.3 Upper Cross Section Limit including Systematics

I convolute likelihood distribution with gaussian for each resonance mass. The width of gaussian is taken as absolute uncertainty in each resonance mass. The equation of convolution is taken as following [7]:

$$L(\grave{\sigma}) = \int_0^\infty L(\sigma)G(\sigma)d\sigma \tag{10}$$

The effects of systematics is presented Fig. 14. The left plot in Fig. 14 shows the cross section limit for qg resonance with including systematic and without systematic. Cross section limits increase by about 30% with systematics uncertainties and mass limit decrease by about $100GeV$. Fractional change between limits for all resonances are shown on the right plot in Fig. 14. The cross section limits vary roughly from 40% at $0.7\,TeV$ to 20% at $3.5\,TeV$. Dijet resonance sensitivity for $10pb^{-1}$ with including systematic uncertainties is illustrated in Fig. 15

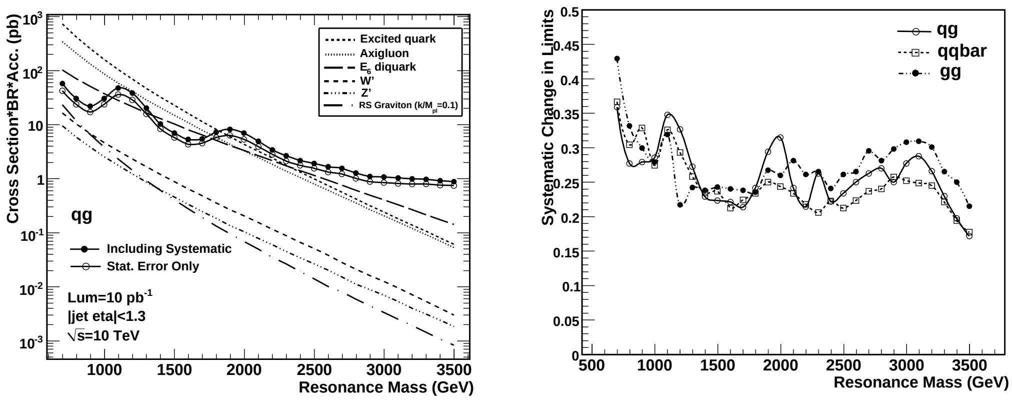

Figure 14: *Left plot*: Comparison of cross section limits for qg resonance. *Right plot*: Fractional change on limit with including systematics.

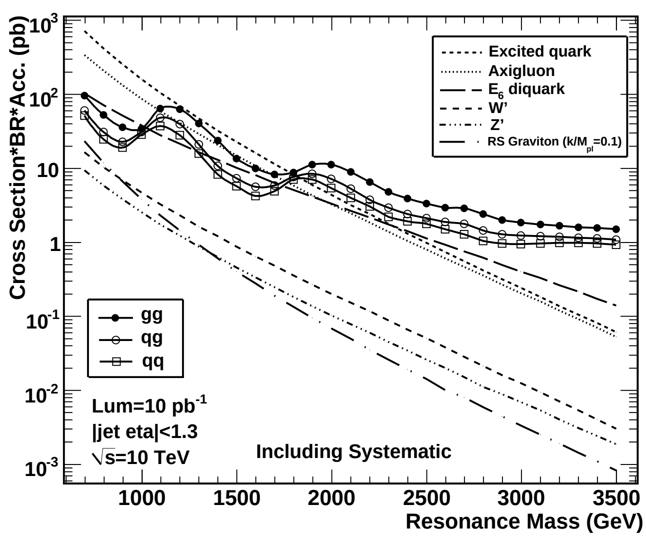

Figure 15: Dijet resonance sensitivity for $10pb^{-1}$ with including systematic uncertainties.

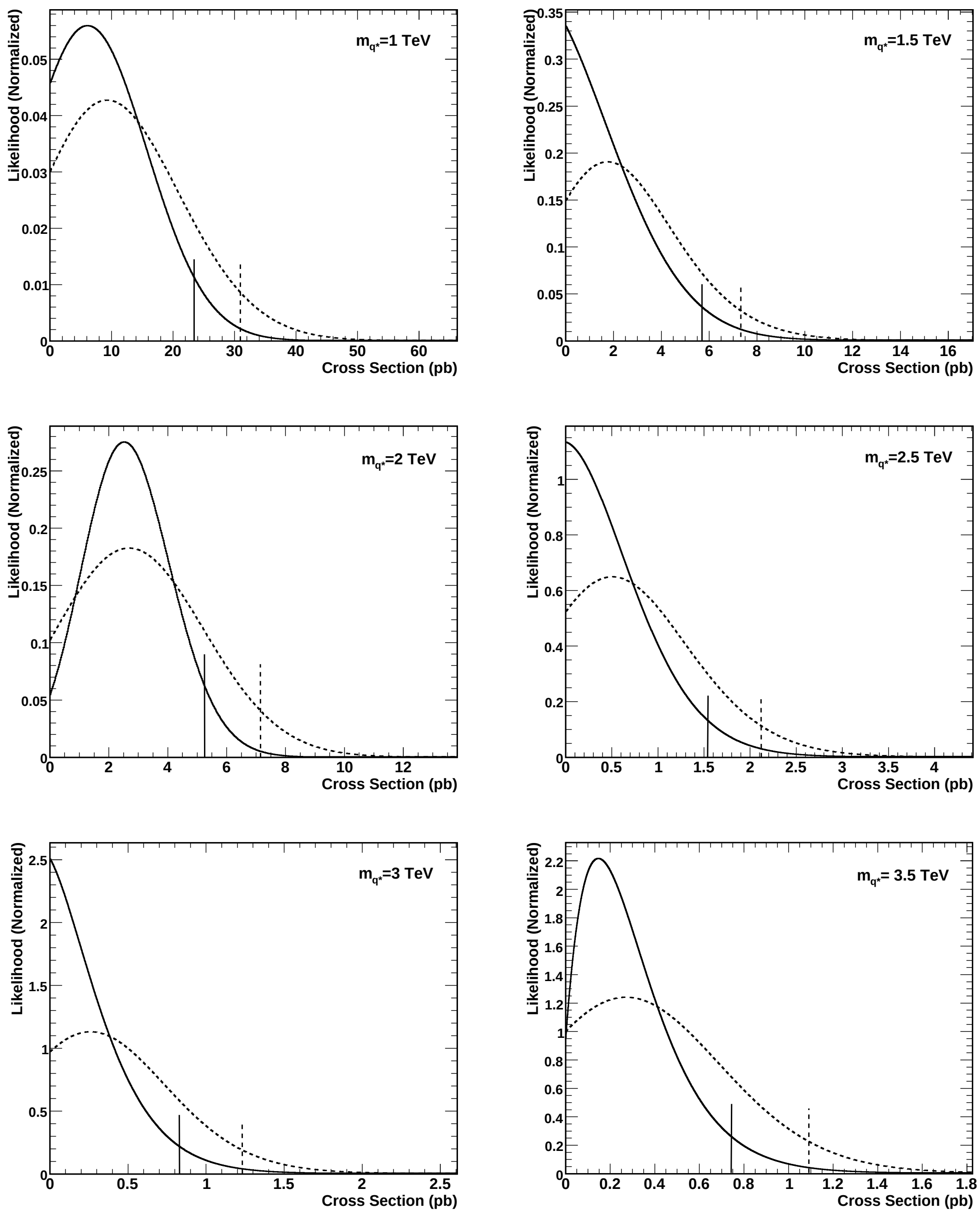

Figure 16: Likelihood distribution with %95 C.L. cross section limit at various excited quark resonance masses including systematics. Solid line is %95 C.L. cross section limit with statistical error only. Dashed line shows %95 C.L. cross section limit with including systematics.

4 Conclusion

We exclude at 95% C.L. new particles in mass region for which the theory curve lies above our upper limit for the appropriate pair of partons. For axigluons (or colorons) we use our limits on qq resonances to exclude the mass range $0.7 < M(A) < 1.8\,TeV$. For excited quarks we use our limits on qg resonances to exclude the mass range $0.7 < M(q*) < 1.8\,TeV$. For E_6 diquarks we use our limits on qq resonances to exclude the mass range $0.7 < M(D) < 1.0\,TeV$, and $1.3 < M(D) < 1.7\,TeV$. The systematic uncertainties in this analysis reduced the highest excluded mass roughly $0.1\,TeV$ for each type of new particles. The comparison of limits between our result and CDF published result [15] can be seen in Table. 2.

Model Name	95% C.L. Excluded Mass (TeV)	
	CMS ($10\,pb^{-1}$, $\sqrt{s} = 10\,TeV$)	CDF ($1\,fb^{-1}$, $\sqrt{s} = 1.96\,TeV$)
Excited Quark	$M(q*) < 1.8\,TeV$	$M(q*) < 0.87\,TeV$
Axigluon, Coloron	$M(A) < 1.8\,TeV$	$M(A) < 1.25\,TeV$
E_6 Diquark	$M(D) < 1.0\,TeV$, $1.3 < M(D) < 1.7\,TeV$	$M(D) < 0.63\,TeV$

Table 2: 95% C.L. Excluded Mass for various models

Mass	95% C.L. $\sigma \cdot B$ (pb)		
(TeV)	qq	qg	gg
0.7	51	60	95
0.8	25	31	52
0.9	19	23	35
1.0	28	31	34
1.1	37	48	64
1.2	28	39	63
1.3	16	21	40
1.4	8.3	11	23
1.5	5.7	7.3	14
1.6	4.2	5.6	9.9
1.7	4.9	5.8	8.3
1.8	6.9	7.6	8.8
1.9	7.1	8.4	11
2.0	5.4	7.2	11
2.1	4.0	5.3	9.0
2.2	3.0	3.7	6.4
2.3	2.2	2.9	4.8
2.4	1.9	2.4	3.9
2.5	1.8	2.1	3.3
2.6	1.5	1.9	2.9
2.7	1.3	1.8	2.9
2.8	1.0	1.5	2.4
2.9	0.95	1.3	2.0
3.0	0.94	1.2	1.8
3.1	0.95	1.2	1.7
3.2	0.97	1.2	1.6
3.3	0.97	1.2	1.6
3.4	0.95	1.1	1.5
3.5	0.92	1.1	1.5

Table 3: As a function of new particle mass we list our 95% C.L. upper limit on cross section times branching ratio for narrow resonances decaying to dijets

References

[1] Kenneth Lane and Stephen Mrenna, Phys. Rev. D67, 115011(2003), hep-ph/0210299.

[2] E.H.Simmons, Phys. Rev. D55 (1997) 1678.

[3] U.Baur, I.Hinchliffe and D.Zeppenfeld, Int.J.Mod.Phys.A2 (1987) 1285.

[4] E.Eichten, I.Hinchliffe, K.D.Lane and C.Quigg, Rev.Mod.Phys.56 (1984) 579.

[5] J.L.Hewett and T.G.Rizzo, Phys.Rept.183 (1989) 193.

[6] L.Randall and R.Sundrum, Phys.Rev.Lett.83 (1999) 4690.

[7] J.Conway, CDF Pub.Note (2005) 6428

[8] G. P. Salam and G. Soyez, JHEP 0705:086 (2007).

[9] CMS Collaboration, CMS Physics Analysis Summary JME-07-002 (2008). at http://cms-physics.web.cern.ch/cms-physics/public/JME-07-002-pas.pdf .

[10] CMS Collaboration, CMS Physics Analysis Summary JME-07-003 (2008). at http://cms-physics.web.cern.ch/cms-physics/public/JME-07-003-pas.pdf .

[11] T. Sjostrand, L. Lonnblad, S. Mrenna, hep-ph/0108264.

[12] R. Adolphi et al., CMS Collaboration, JINST 3:S08004 (2008).

[13] CMS Collaboration, Physics TDR Volume I, CERN-LHCC-2006-001.

[14] M.Cardaci et all.,CMS AN-2007/039, (2007)

[15] T.Aaltonen et al., hep-ex/08124036, (2008)